Intent Sharing in Cooperative Maneuvering: Theory and Experimental Evaluation

Hao M. Wang, Sergei S. Avedisov, *Member, IEEE*, Onur Altintas, and Gábor Orosz, *Senior Member, IEEE*

***Abstract*— Intent sharing is a class of cooperation enabled by vehicle-to-everything (V2X) communication, which allows for information exchange between road users about their intended future behaviors. In this paper, we propose a generalized representation of vehicles' motion intent from a dynamical systems viewpoint. Based on this, we extend the framework of conflict analysis such that intent information can be interpreted in real time to assist the decision-making of intent-receiving vehicles and ensure conflict-free maneuvers. We create intent messages using commercially available V2X radios, and demonstrate experimentally the benefits of sharing intent in cooperative maneuvering. Experiments are performed on a test track where intent-based on-board decision assistance is provided to human drivers in merge scenarios. The experimental results reveal significant benefits of intent sharing in enhancing vehicle safety and time efficiency. Furthermore, we test intent messages on public roads and evaluate the performance in terms of packet delivery ratio. The data collected on public highways are fed into numerical simulations to investigate the effects of intent transmission conditions on conflict resolution.**

***Index Terms*— V2X communication, intent sharing, connected and automated vehicles, conflict analysis.**

I. Introduction

RECENT advances in vehicular automation, on-board sensing, and vehicle-to-everything (V2X) communication exhibit great potential to improve the efficiency and safety of transportation systems by resolving conflicts between road users in a cooperative manner [1]. Envisioning an environment consisting of fully automated agents, prior studies show that V2X communication can allow the negotiation between vehicles about their future maneuvers using maneuver coordination messages [2], [3]. A plethora of control strategies may be applied to realize such cooperative maneuvers, including virtual platooning [4], optimal control [5], [6], [7], reachability analysis [8], [9], [10], and reinforcement learning [11].

In the near future, however, having a fully automated environment looks unrealistic. Traffic environments in the forthcoming decades are expected to be dominated by mixed-autonomy, where vehicles of different automation degrees and cooperation classes share the roadways [12], [13]. In such mixed environments, negotiating future trajectories may oftentimes be infeasible, and the cooperation between vehicles may stay within two classes: status sharing and intent sharing. In status sharing, connected vehicles share status information such as position and velocity, whereas in intent sharing, the information regarding future motion is exchanged (e.g., velocity and acceleration bounds over a time horizon). Status sharing is well-standardized. Examples include basic safety messages (BSMs) [14] and cooperative awareness messages (CAMs) [15]. Although status information allows a vehicle to understand its instantaneous surroundings, it can lead to overly conservative decisions and abrupt actions due to the absence of foresight into the future. On the other hand, intent sharing, an emerging form of cooperation, is attracting increasing attention. Intent information can benefit a vehicle's decision making and control design by providing a more accurate prediction for the evolution of future environments.

A. Related Work

In the literature of intent-enhanced maneuver coordination, many works focus on scenarios where driving intent of other vehicles is estimated from the available status information, while the exact intent is not shared directly via communication. Estimation techniques include optimization [16], statistical inference [17], and learning based strategies [18]. However, such estimation can be inaccurate and may not always be completed in a timely manner due to large computational load. Instead of estimating intent, we focus on V2X communication-based intent sharing, which enables more detailed and precise interpretation of vehicle intent.

Standardization of intent sharing is currently in progress. For example, the Society of Automotive Engineers (SAE) is establishing maneuver sharing and coordination service [19], while the European Telecommunications Standards Institute (ETSI) is standardizing maneuver coordination service [20]. These standards are still under development, and intent messages have not been created and field-tested so far. On the other hand, a noticeable amount of theoretical research has been triggered by the ongoing standardization. For instance, [21] and [22] studied maneuver coordination messages which contained the planned and desired trajectories (as polynomials of time) for automated vehicles. From a communication

Manuscript received 8 October 2023; revised 31 January 2024; accepted 18 March 2024. Date of publication 4 April 2024; date of current version 29 August 2024. This work was supported by Toyota Motor North America Research and Development - InfoTech Labs, Mountain View, CA, USA. The Associate Editor for this article was S.-H. Kong. *(Corresponding author: Hao M. Wang.)*

Hao M. Wang is with the Department of Mechanical Engineering, University of Michigan, Ann Arbor, MI 48109 USA (e-mail: haowangm@umich.edu).

Sergei S. Avedisov and Onur Altintas are with Toyota Motor North America Research and Development–InfoTech Labs, Mountain View, CA 94043 USA (e-mail: sergei.avedisov@toyota.com; onur.altintas@toyota.com).

Gábor Orosz is with the Department of Mechanical Engineering and the Department of Civil and Environmental Engineering, University of Michigan, Ann Arbor, MI 48109 USA (e-mail: orosz@umich.edu).

Digital Object Identifier 10.1109/TITS.2024.3379994

perspective, [23] studied generation rules of such messages, while [24] evaluated the impact of maneuver coordination in large-scale traffic via simulations. Also, a framework is proposed in [25] where vehicles' intended trajectories are communicated with B-spline representation in a fully automated car-following scenario. Considering mixed traffic, a tool called conflict analysis was developed in our previous works [26], [27], [28] to resolve maneuver conflicts. A vehicle's intent was defined as restricted bounds of kinematic variables (e.g., acceleration and velocity) over a future time horizon. Such conflict analysis tool interprets the received V2X information using a conflict chart, where the state space is partitioned into domains of qualitatively different behaviors in terms of conflict prevention.

These prior studies on intent sharing are limited to theory, and a clear gap exists on evaluating the benefits of intent in the real world. To the best of our knowledge, no previous work has evaluated experimentally the benefits of intent sharing in conflict resolution, and the corresponding communication requirements for intent-sharing messages have been unclear. This paper provides a first effort to address this gap.

B. Contributions of This Paper

We first propose a generalized representation of vehicle intent from the perspective of input/output relationship in dynamical systems. Such representation allows us to describe the intent of vehicles possessing different automation levels. We then implement, test, and systematically evaluate intent sharing using commercially available V2X communication devices on real production vehicles. We extend the aforementioned conflict analysis framework such that the information encoded in status and intent messages can be tailored for both automated and human-driven vehicles. This enables personalized decision-making assistance that considers user-based preferences for conflict prevention during cooperative maneuvers.

Using merge scenarios as an application example, we test intent sharing for conflict resolution at a closed test track where a main road vehicle approaches a merge zone while sending both status and intent messages. These V2X messages are received by a human-driven vehicle seeking to join the main road. We use the extended conflict analysis to assist the decision-making of the merging vehicle. Through experiments, we validate an on-board warning system for human drivers that enhances maneuver safety. Results show that compared to status sharing, receiving additional intent messages can substantially mitigate a human driver's decision inefficiency, leading to more time-efficient, yet still safe, maneuvers. Such merits are quantified by a proposed metric. To further investigate intent sharing in the real world, we test intent messages on public highways. Performance is evaluated via the packet delivery ratio, i.e., the percentage of intent packets received out of those have been sent. We feed the collected data into numerical simulations to study the effects of communication conditions (e.g., intent message sending rate, intent horizon, and packet drops) on the benefits of intent sharing in conflict resolution.

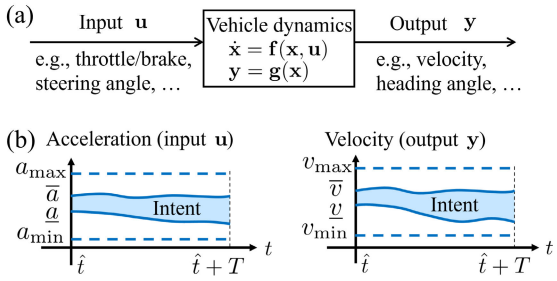

Fig. 1. Modeling vehicle intent from dynamical systems viewpoint. (a) Diagram showing the input/output representation of a vehicle's motion. (b) Conceptual illustration of a vehicle's longitudinal motion intent.

This paper extends the initial results reported in our conference paper [29]. Compared to it, major contributions of this paper are threefold. (i) We generalize the representation of vehicle intent from a dynamical systems viewpoint and establish the corresponding framework of conflict analysis. (ii) We perform test-track experiments on intent-based conflict analysis to demonstrate personalized on-board decision assistance. (iii) We collect and utilize real highway data to evaluate the benefits of intent sharing under different transmission conditions and imperfect communication. Insights from this analysis may benefit the on-going standardization and future real-world deployment.

The remainder of this paper is organized as follows. In Section II we define vehicle motion intent. In Section III we establish the extended conflict analysis framework. In Section IV we implement intent messages and test intent-based conflict analysis experimentally. In Section V, highway data is used to investigate the benefits of sharing intent. Section VI concludes the paper and discusses future directions.

II. Defining Motion Intent of Vehicles

To provide a rigorous definition of vehicle intent, we consider a vehicle's motion from a dynamical systems viewpoint. As shown in Fig. 1(a), the vehicle's behavior may be described by some observable quantities that we refer to as *outputs*, for example, the vehicle's velocity and the heading angle. Such outputs are influenced by some other quantities called *inputs* that are applied to the vehicle. Examples of inputs are the throttle/brake and steering angle applied by the human driver or set by the autonomous driving system. Note that depending on the fidelity of the model describing the vehicle's motion, different quantities may be considered as inputs and outputs. Based on this, we represent the vehicle's motion intent by the bounded domains of inputs and outputs over a time horizon; see Fig. 1(b) for a conceptual illustration using the acceleration as input and the velocity as output. Note that the domains specified in intent are more restricted than the vehicle's physical behavior limits since uncertainties are reduced when anticipating the vehicle's future maneuver. A formal definition of such vehicle intent is given below.

Definition 1: A vehicle's motion intent is represented by the restricted domains $\mathbf{u}(t) \in [\underline{\mathbf{u}}(t), \overline{\mathbf{u}}(t)]$ *and* $\mathbf{y}(t) \in [\underline{\mathbf{y}}(t), \overline{\mathbf{y}}(t)]$ *of the input and output over the time period* $t \in [\hat{t}, \hat{t}+T]$, *where*

$\hat{t}$ is the time when the intent is generated, and T is the intent horizon. The vectors $\underline{\mathbf{u}}$, $\overline{\mathbf{u}}$, $\underline{\mathbf{y}}$, and $\overline{\mathbf{y}}$ collect the lower and upper bounds of the input vector $\mathbf{u}$ and the output vector $\mathbf{y}$, and these bounds can be time-dependent. ■

It is emphasized that according to Definition 1, a vehicle's intent can be compactly encoded into the input/output bounds, enabling an efficient implementation of intent sharing communication. Note that such intent information does not specify the intent sender's vehicle dynamics; see Fig. 1(a). However, the encoded input bounds and output constraints can be interpreted by an intent receiver using an appropriately chosen dynamical model, which allows the calculation of possible future trajectories of the intent sender in continuous time. We remark that Definition 1 is kept general such that one can describe a vehicle's intent for different scenarios under a unified framework, by selecting appropriate input/output quantities. Below we provide a more specific definition for a vehicle's longitudinal motion intent based on Definition 1, which considers acceleration as input and velocity as output along a planned path; see Fig. 1(b) for an illustration.

Definition 2: A vehicle's longitudinal motion intent is represented by a lane index I, a restricted acceleration (input) domain $u(t) \in [\underline{a}(t), \overline{a}(t)]$ and velocity (output) domain $v(t) \in [\underline{v}(t), \overline{v}(t)]$ over the time period $t \in [\hat{t}, \hat{t}+T]$, where $\hat{t}$ is the time when this intent is generated, T is the intent horizon. Also, $a_{\min} \le \underline{a}(t) \le \overline{a}(t) \le a_{\max}$ and $v_{\min} \le \underline{v}(t) \le \overline{v}(t) \le v_{\max}$ where $a_{\min}$, $a_{\max}$, $v_{\min}$, and $v_{\max}$ denote the physical acceleration and velocity limits. ■

For instance, in a highway driving scenario, an intent message may convey the information that for the next $T = 8$ [s], the vehicle will be traveling on the left-most lane (i.e., $I = 1$) while having its velocity between $\underline{v}(t) \equiv 29$ [m/s] and $\overline{v}(t) \equiv 32$ [m/s], and acceleration between $\underline{a}(t) \equiv -0.7$ [m/s^2] and $\overline{a}(t) \equiv 0.9$ [m/s^2]. It will be demonstrated below experimentally that the intent given by Definition 2 can be decoded to predict the intent sender's future behaviors using a simple first-principle model of longitudinal dynamics.

We remark that the intent of an automated vehicle may be given by specifying its future trajectory [21], [22], [25]. However, a major advantage of our representation is the capability of encoding uncertainties into motion intent (through input/output bounds) in an easy-to-interpret fashion. Thus, Definitions 1 and 2 can be implemented for vehicles possessing various automation degrees. For a connected automated vehicle, such intended input bounds and output constraints may be extracted from its on-board motion planner that prescribes the vehicle's future behaviors. On the other hand, for a connected human-driven vehicle, the intent bounds may be determined in a data-driven manner for a specific human driver involved in similar traffic scenarios. Section IV discusses in detail the implementation of intent sharing communication. We also remark that Definition 2 can be easily extended to include lane changes by specifying lane indices that correspond to different time periods. Alternatively, lateral motion can be incorporated into the definition of intent, by specifying the steering angle as an input, in accordance with Definition 1.

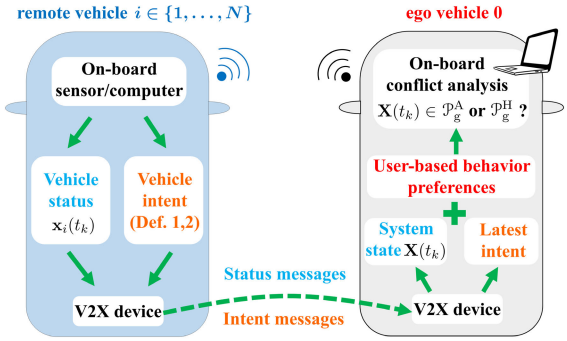

Fig. 2. Schematic diagram of on-board conflict analysis that provides real-time decision assistance to the ego vehicle based on the remote vehicles' status and intent messages.

With the definition of vehicle intent, the next section provides theoretical preparation for the application of intent sharing for conflict resolution in cooperative maneuvering.

III. Conflict Analysis

In this section, we generalize the framework of conflict analysis, originally proposed in our previous work [26], by considering multiple vehicles with general dynamical models and general cooperative driving scenarios. Under this extension, the received V2X messages can be interpreted in a personalized manner for both automated and human-driven vehicles considering their user-determined behavior preferences. Fig. 2 shows an illustration of the intent-based conflict analysis that we develop in this section. This generalized framework is then applied to investigate conflicts in a merge scenario.

A. Intent-Based Conflict Analysis

Consider a cooperative maneuver involving an ego vehicle indexed 0, and N remote vehicles indexed $1, \ldots, N$, whose dynamics are modeled by:

$$\begin{aligned} \dot{\mathbf{x}}_i(t) &= \mathbf{f}_i(\mathbf{x}_i(t), \mathbf{u}_i(t)), \\ \mathbf{y}_i(t) &= \mathbf{g}_i(\mathbf{x}_i(t)), \qquad i = 0, 1, \ldots, N. \end{aligned} \tag{1}$$

Here the dot denotes time derivative, $\mathbf{x}_i \in \Omega_i \subseteq \mathbb{R}^n$ is the state of vehicle i, $\mathbf{u}_i \in \mathbb{R}^m$ is the input, $\mathbf{y}_i \in \mathbb{R}^q$ is the output, and $\mathbf{f}_i : \Omega_i \times \mathbb{R}^m \to \Omega_i$, $\mathbf{g}_i : \Omega_i \to \mathbb{R}^q$ are continuous functions. Each vehicle $i \in \{0, 1, \ldots, N\}$ is subject to

$$\mathbf{u}_i(t) \in [\mathbf{u}_{\min,i}, \mathbf{u}_{\max,i}], \quad \mathbf{y}_i(t) \in [\mathbf{y}_{\min,i}, \mathbf{y}_{\max,i}], \quad \forall t, \tag{2}$$

where $\mathbf{u}_{\min,i}, \mathbf{u}_{\max,i} \in \mathbb{R}^m$ and $\mathbf{y}_{\min,i}, \mathbf{y}_{\max,i} \in \mathbb{R}^q$ contain the (constant) lower and upper bounds for the input and output, imposed by the vehicle's physical behavior limits.

From the perspective of the ego vehicle 0, the remote vehicles $1, \ldots, N$ are not controllable. That is, we cannot prescribe the inputs $\mathbf{u}_1, \ldots, \mathbf{u}_N$, nor do we have the knowledge about their exact values. However, the remote vehicles' physical behavior limits in (2) are assumed to be known to the ego vehicle based on general knowledge of vehicle capabilities and traffic rules. Moreover, the remote vehicles may share their

status $\mathbf{x}_i$ and intent (cf. Definition 1) with the ego vehicle at given time instants. For example, knowing the intent of a remote vehicle $i \in \{1, \ldots, N\}$ generated at time $\hat{t}$, in addition to (2), imposes the following input and output bounds:

$$\mathbf{u}_i(t) \in [\underline{\mathbf{u}}_i(t), \overline{\mathbf{u}}_i(t)], \quad \mathbf{y}_i(t) \in [\underline{\mathbf{y}}_i(t), \overline{\mathbf{y}}_i(t)], \quad t \in [\hat{t}, \hat{t}+T], \tag{3}$$

where the conditions $\mathbf{u}_{\min,i} \leq \underline{\mathbf{u}}_i(t) \leq \overline{\mathbf{u}}_i(t) \leq \mathbf{u}_{\max,i}$ and $\mathbf{y}_{\min,i} \leq \underline{\mathbf{y}}_i(t) \leq \overline{\mathbf{y}}_i(t) \leq \mathbf{y}_{\max,i}$ hold (element-wise). Given the remote vehicle's current status $\mathbf{x}_i$, its future evolution can be predicted from (1) under the constraints (2)-(3). We leave the details of communication setups for the next subsection, while here we present the main idea of conflict analysis.

We define the overall state of the system (1) as

$$\mathbf{X} := \begin{bmatrix} \mathbf{x}_0 \\ \mathbf{x}_1 \\ \vdots \\ \mathbf{x}_N \end{bmatrix} \in \Omega := \Omega_0 \times \Omega_1 \times \ldots \times \Omega_N, \tag{4}$$

where Ω contains the states of interest when reasoning about conflicts between vehicles. We formally describe a conflict-free maneuver using the proposition

$$P := \{\forall t, \mathbf{X}(t) \notin \Omega^* \subseteq \Omega\}, \tag{5}$$

where Ω^* is the set that the states $\mathbf{X}(t)$ must avoid for all time t to ensure that a conflict never occurs during the maneuver. Note that encoding conflict conditions in the set Ω^* is a general representation which can be used to describe conflicts in a multitude of traffic scenarios.

Our goal is to ensure that the proposition P holds, by assisting the maneuver of the ego vehicle 0 while considering the environmental uncertainty coming from the remote vehicles. Such assistance may be provided at the decision level (e.g., whether the ego vehicle is able to merge ahead of an approaching remote vehicle without a conflict) and/or at the control level (e.g., what control input $\mathbf{u}_0(t)$ should be used to execute the corresponding decision). In this study, we focus on providing decision-level assistance to the ego vehicle (which may be either automated or human-driven), while leaving the control-level assistance for future work. To provide a personalized decision assistance, we consider the ego vehicle's user-based behavior preferences, modeled as input bounds and output constraints:

$$\mathbf{u}_0(t) \in [\underline{\mathbf{u}}_0(t), \overline{\mathbf{u}}_0(t)], \quad \mathbf{y}_0(t) \in [\underline{\mathbf{y}}_0(t), \overline{\mathbf{y}}_0(t)], \tag{6}$$

similar to the intent Definition 1. We assume that these bounds cover the whole time span of the ego vehicle's maneuver.

For an automated ego vehicle, such preference may be preset according to different metrics (e.g., passenger comfort and energy efficiency). When the ego vehicle is human-driven, these preference bounds may be extracted from specific human drivers' historical data when they were involved in similar maneuvers. Notice that for an automated ego vehicle, the behavior preference (6) represents the constraints in designing control strategies for completing a given maneuver. For the human-driven case, however, such preference represents the uncertainty in a human driver's behavior when performing the maneuver. In this case we assist the human driver's decision, but the vehicle is maneuvered by the driver.

With the ego vehicle's behavior preference and the remote vehicles' behavior uncertainty in mind, proposition P in (5) can be decomposed into three cases:

(i) No-conflict case: Independent of the motion of remote vehicles $1, \ldots, N$, the ego vehicle 0 is able to perform a conflict-free maneuver under its behavior preference.
(ii) Uncertain case: Depending on the motion of remote vehicles $1, \ldots, N$, the ego vehicle 0 may be able to perform a conflict-free maneuver under its behavior preference.
(iii) Conflict case: Independent of the motion of remote vehicles $1, \ldots, N$, the ego vehicle 0 is not able to perform a conflict-free maneuver under its behavior preference.

These three cases correspond to three pairwise disjoint sets within the set Ω. Depending on whether the ego vehicle 0 is automated or human-driven, different expressions are required for these sets. For an automated ego vehicle, we have

$$\mathcal{P}_{\mathrm{g}}^{\mathrm{A}} := \{\mathbf{X} \in \Omega | \forall \mathbf{u}_1(t), \ldots, \mathbf{u}_N(t), \exists \mathbf{u}_0(t), P\}, \tag{7}$$

$$\mathcal{P}_{\mathrm{y}}^{\mathrm{A}} := \{\mathbf{X} \in \Omega | (\exists \mathbf{u}_1(t), \ldots, \mathbf{u}_N(t), \forall \mathbf{u}_0(t), \neg P) \wedge (\exists \mathbf{u}_1(t), \ldots, \mathbf{u}_N(t), \exists \mathbf{u}_0(t), P)\}, \tag{8}$$

$$\mathcal{P}_{\mathrm{r}}^{\mathrm{A}} := \{\mathbf{X} \in \Omega | \forall \mathbf{u}_1(t), \ldots, \mathbf{u}_N(t), \forall \mathbf{u}_0(t), \neg P\}, \tag{9}$$

where the symbol $\neg$ means "negation" and $\wedge$ means "and". The inputs $\mathbf{u}_0, \mathbf{u}_1, \ldots, \mathbf{u}_N$ are subject to their corresponding bounds imposed by the physical behavior limits (2), the intent (3) of remote vehicles, and the behavior preference (6) of ego vehicle. The superscript "A" corresponds to the ego vehicle being automated, while the subscripts "g", "y", and "r" correspond to the convention of using green, yellow, and red colors to visualize the no-conflict, uncertain, and conflict sets [26]. If the ego vehicle is human-driven, we have

$$\mathcal{P}_{\mathrm{g}}^{\mathrm{H}} := \{\mathbf{X} \in \Omega | \forall \mathbf{u}_1(t), \ldots, \mathbf{u}_N(t), \forall \mathbf{u}_0(t), P\}, \tag{10}$$

$$\mathcal{P}_{\mathrm{y}}^{\mathrm{H}} := \{\mathbf{X} \in \Omega | (\exists \mathbf{u}_1(t), \ldots, \mathbf{u}_N(t), \exists \mathbf{u}_0(t), \neg P) \wedge (\exists \mathbf{u}_1(t), \ldots, \mathbf{u}_N(t), \forall \mathbf{u}_0(t), P)\}, \tag{11}$$

$$\mathcal{P}_{\mathrm{r}}^{\mathrm{H}} := \{\mathbf{X} \in \Omega | \forall \mathbf{u}_1(t), \ldots, \mathbf{u}_N(t), \exists \mathbf{u}_0(t), \neg P\}, \tag{12}$$

where the superscript "H" is used for the human-driven case.

We emphasize that the no-conflict set $\mathcal{P}_{\mathrm{g}}^{\mathrm{A}}$ in (7) requires the existence of an input for the automated ego vehicle (i.e., $\exists \mathbf{u}_0$), which steers the system state $\mathbf{X}$ such that the proposition P remains true. In contrast, the no-conflict set $\mathcal{P}_{\mathrm{g}}^{\mathrm{H}}$ in (10) requires the proposition P to hold for any input of the human-driven ego vehicle (i.e., $\forall \mathbf{u}_0$) under the behavior preference (6). Such difference accounts for the behavior uncertainty associated with the ego vehicle's human driver, while considering that an automated counterpart can execute a prescribed input without significant uncertainty. One may observe similar difference in the conflict sets $\mathcal{P}_{\mathrm{r}}^{\mathrm{A}}$ and $\mathcal{P}_{\mathrm{r}}^{\mathrm{H}}$. These yield the relationships

$$\mathcal{P}_{\mathrm{g}}^{\mathrm{A}} \supseteq \mathcal{P}_{\mathrm{g}}^{\mathrm{H}}, \quad \mathcal{P}_{\mathrm{r}}^{\mathrm{A}} \subseteq \mathcal{P}_{\mathrm{r}}^{\mathrm{H}}. \tag{13}$$

That is, under the behavior uncertainty of ego vehicle's human driver, the no-conflict set shrinks while the conflict set enlarges compared to the automated case. We remark that for both the automated and human-driven cases, the two predicates of the uncertain set $\mathcal{P}_{\mathrm{y}}^{*}$ negate those of the no-conflict set $\mathcal{P}_{\mathrm{g}}^{*}$ and

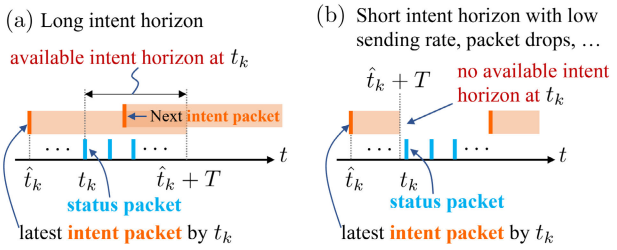

Fig. 3. Visualizing packet receiving timing of V2X messages. (a) When intent packet has sufficient horizon. (b) When intent packet has short horizon while being sent with a low rate or when packet drops occur.

conflict set $\mathcal{P}_{\mathrm{r}}^{*}$ (where "$*$" denotes either "A" or "H"). For human-driven case (10)-(12), we have

$$(\exists \mathbf{u}_1(t), \ldots, \mathbf{u}_N(t), \exists \mathbf{u}_0(t), \neg P) \iff \neg(\forall \mathbf{u}_1(t), \ldots, \mathbf{u}_N(t), \forall \mathbf{u}_0(t), P), \tag{14}$$

$$(\exists \mathbf{u}_1(t), \ldots, \mathbf{u}_N(t), \forall \mathbf{u}_0(t), P) \iff \neg(\forall \mathbf{u}_1(t), \ldots, \mathbf{u}_N(t), \exists \mathbf{u}_0(t), \neg P), \tag{15}$$

which explains why the sets $\mathcal{P}_{\mathrm{g}}^{\mathrm{H}}$, $\mathcal{P}_{\mathrm{y}}^{\mathrm{H}}$, and $\mathcal{P}_{\mathrm{r}}^{\mathrm{H}}$ are mutually disjoint and $\mathcal{P}_{\mathrm{g}}^{\mathrm{H}} \cup \mathcal{P}_{\mathrm{y}}^{\mathrm{H}} \cup \mathcal{P}_{\mathrm{r}}^{\mathrm{H}} = \Omega$. Similar relationships hold for the sets $\mathcal{P}_{\mathrm{g}}^{\mathrm{A}}$, $\mathcal{P}_{\mathrm{y}}^{\mathrm{A}}$, and $\mathcal{P}_{\mathrm{r}}^{\mathrm{A}}$.

By checking which subset of Ω the system state $\mathbf{X}$ is currently located at, one can assist the ego vehicle to identify the opportunity in completing a conflict-free maneuver, resulting in safe and efficient decision. Note that such checking is made possible by the status and intent of the remote vehicles shared via V2X communication. The corresponding communication setup is provided in the next subsection.

B. Communication Setup

We consider that all vehicles are equipped with V2X devices. The ego vehicle may acquire information regarding the remote vehicles' motion via status sharing and intent sharing. In status sharing, the ego vehicle 0 receives status information from the remote vehicles $1, \ldots, N$ at discrete time moments t_k, $k = 0, 1, \ldots$, i.e., it obtains $[\mathbf{x}_1(t_k)^\top, \ldots \mathbf{x}_N(t_k)^\top]^\top$. Here, for simplicity, we assume that the reception of status messages from all N remote vehicles is synchronized at each t_k. Due to the discrete nature of status information, the ego vehicle has the accurate knowledge of system state $\mathbf{X}$ at times t_k only. In intent sharing, the remote vehicles transmit their intent messages at discrete time moments according to Definition 1. Similar to status sharing, we assume that the reception of intent messages are synchronized for all N remote vehicles.

For both status and intent packets, the transmission time delay is assumed to be negligible such that a message is delivered immediately to the ego vehicle once generated from the remote vehicle. For analysis with time delays, we refer the readers to our previous work [28]. However, the two types of messages (status and intent) may be transmitted with different sending rates, and therefore, they may not arrive at the ego vehicle's V2X port in a synchronized fashion. A conceptual visualization of the message reception timing is shown in Fig. 3(a). For simplicity of notation, we avoid introducing a new index of intent messages, but simply use $\hat{t}_k \le t_k$ to denote the latest time when the intent packets were received by the ego vehicle, at the status receiving time t_k. This corresponds to the notation used in (3) if one substitutes $\hat{t}$ with $\hat{t}_k$ for all remote vehicles.

At each time t_k, the available intent information, that the ego vehicle may use to predict the remote vehicle's future trajectory, covers the time horizon $[t_k, \hat{t}_k + T]$; see Fig. 3(a). If intent packets are designed with a short horizon T, while subject to low sending rate and/or to packet drops, then $t_k \ge \hat{t}_k + T$ may occur; see Fig. 3(b). In this case, the information in the latest intent packet already expires at t_k and may not be used to facilitate the ego vehicle's prediction. This suggests that a sufficient intent horizon together with appropriate communication conditions are needed to secure a satisfactory performance of intent sharing. Detailed evaluation of these communication factors are given in Section V via real highway data.

With this communication setup, one is able to check the system state $\mathbf{X}$ at each time t_k while using the latest (available) intent information. If $\mathbf{X}(t_k) \in \mathcal{P}_{\mathrm{g}}^{\mathrm{A}}$ or $\mathbf{X}(t_k) \in \mathcal{P}_{\mathrm{g}}^{\mathrm{H}}$ (depending on whether the ego vehicle is automated or human-driven), then a conflict is guaranteed not to happen, and the ego vehicle may confidently initiate such a maneuver according to its behavior preference. Otherwise, the ego vehicle should not execute the maneuver to prevent potential conflicts caused by the behavior uncertainties of the remote and the ego vehicles. In the next subsection, we apply this conflict analysis framework to a merge scenario and develop an efficient algorithm to check whether $\mathbf{X}(t_k) \in \mathcal{P}_{\mathrm{g}}^{\mathrm{A}}$ or $\mathbf{X}(t_k) \in \mathcal{P}_{\mathrm{g}}^{\mathrm{H}}$.

C. Conflict Analysis for a Merge Scenario

As an application of intent-based conflict analysis, we focus on the example of a merge scenario illustrated in Fig. 4(a). This maneuver is selected because it is one of the most challenging driving scenarios that frequently involves conflicts. Nevertheless, the results of the following analysis can be applied to a much broader set of conflict scenarios, such as intersections, unprotected left/right turns, and roundabouts.

In Fig. 4(a), the blue remote vehicle 1 is approaching a merge zone (yellow rectangle) while traveling along the main road. In the meantime, the white ego vehicle 0 is attempting to merge onto the main road. The conflict zone (red rectangle) is located towards the end of the merge zone. A conflict occurs when the two vehicles appear simultaneously inside the conflict zone, even partially. Fig. 4(b) shows a generalized model for this scenario, while considering the vehicles' longitudinal dynamics only. We place the origin at the entry point of the conflict zone and use L to denote the conflict zone length. The front bumper positions of the vehicles are denoted by r_0 and r_1, and the corresponding velocities are v_0 and v_1. The same vehicle length ℓ is assumed for both vehicles and we define the variable $s := L + \ell$.

For simplicity, we model the vehicles' longitudinal dynamics while neglecting rolling resistance and air drag:

$$\begin{aligned} \dot{r}_i(t) &= -v_i(t), \\ \dot{v}_i(t) &= u_i(t), \qquad i = 0, 1. \end{aligned} \tag{16}$$

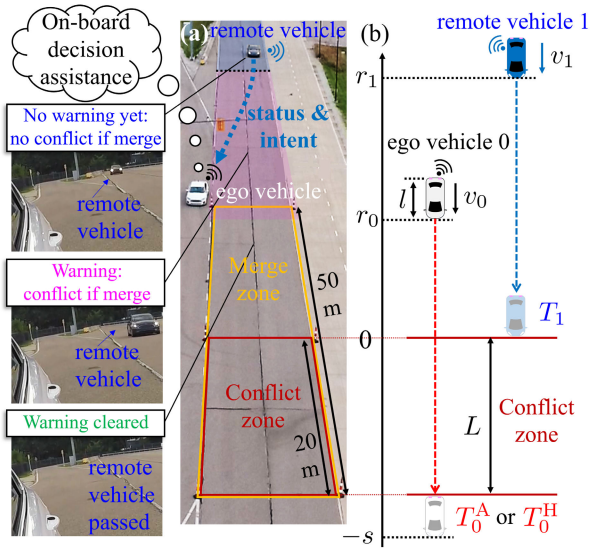

Fig. 4. Validating intent sharing cooperation in a merge scenario using real vehicles at Mcity test track. (a) Experiments where intent-based conflict analysis provides on-board decision assistance to an ego vehicle attempting to merge. The rear mirror views of the ego vehicle are shown in the left column. (b) A generalized model of the merge scenario.

TABLE I
PARAMETER VALUES USED IN THE EXPERIMENTS AT MCITY

d	20 [m]	l	5 [m]
$a_{\min,0}$	-4 [m/s^2]	$a_{\min,1}$	-4 [m/s^2]
$a_{\max,0}$	4 [m/s^2]	$a_{\max,1}$	4 [m/s^2]
$v_{\min,0}$	0 [m/s]	$v_{\min,1}$	8 [m/s]
$v_{\max,0}$	15 [m/s]	$v_{\max,1}$	15 [m/s]

Here, u_i is the control input (acceleration) of vehicle i, and the negative sign in front of the velocity corresponds to the fact that vehicles travel towards the negative direction (towards the conflict zone); see Fig. 4(b). The state and output of vehicle i are defined as $\mathbf{x}_i = [r_i \ v_i]^\top$ and $\mathbf{y}_i = v_i$. The physical behavior limits of both vehicles, in terms of the input (acceleration) bounds and output (velocity) constraints, are given as

$$u_i(t) \in [a_{\min,i}, a_{\max,i}], \quad v_i(t) \in [v_{\min,i}, v_{\max,i}], \quad \forall t, \tag{17}$$

cf. (2). Table I gives the corresponding values drawn from the experiments performed at a closed test track; see more details in Section IV. For vehicle i, the set $\Omega_i = [-s, \infty) \times [v_{\min,i}, v_{\max,i}]$ in state space is used to reason about conflict. Hence the overall state of the system (16) is $\mathbf{X} := [\mathbf{x}_0^\top \ \mathbf{x}_1^\top]^\top \in \Omega := \Omega_0 \times \Omega_1$.

We are interested in whether the ego vehicle is able to merge ahead of the remote vehicle without a conflict. Such a conflict-free merge ahead is given by the proposition

$$P := \{\exists t, r_0(t) < -s \wedge r_1(t) = 0\}, \tag{18}$$

which states that by the time the remote vehicle enters the conflict zone, the ego vehicle has passed it; see Fig. 4(b). Here, we exploited the fact that vehicles only move forward during the merge (i.e., r_0 and r_1 are non-increasing functions of time t). Proposition (18) can be converted to the general form (5):

$$P = \{\forall t, \neg (r_0(t) \geq -s \wedge -s \leq r_1(t) \leq 0)\}, \tag{19}$$

see the proof in Appendix A. That is, to ensure a conflict-free merge ahead, the set

$$\Omega^* = [-s, \infty) \times [v_{\min,0}, v_{\max,0}] \times [-s, 0] \times [v_{\min,1}, v_{\max,1}], \tag{20}$$

must be avoided by the system state $\mathbf{X}$. Here, $\mathbf{X} \in \Omega^* \subset \Omega$ describes the scenario when the remote vehicle 1 is inside the conflict zone while the ego vehicle 0 has not yet exited it: it is either in the conflict zone, or has not yet reached the conflict zone. In this case a conflict-free merge ahead is not possible.

Following the communication setup given in the previous subsection, the ego vehicle has access to the system state $\mathbf{X}(t_k)$ at status message receiving times t_k. The available intent information at t_k is encoded in the latest intent message received from the remote vehicle 1 at $\hat{t}_k$:

$$u_1(t) \in [\underline{a}_1(t), \overline{a}_1(t)], \quad v_1(t) \in [\underline{v}_1(t), \overline{v}_1(t)], \quad t \in [t_k, \hat{t}_k + T]; \tag{21}$$

cf. Definition 2 and Fig. 3. For the ego vehicle 0, the behavior preference

$$u_0(t) \in [\underline{a}_0(t), \overline{a}_0(t)], \quad v_0(t) \in [\underline{v}_0(t), \overline{v}_0(t)], \tag{22}$$

holds until it exits the conflict zone, cf. (6). Fig. 6(a)-(b) show an example of such preference bounds associated with a human driver performing a merge maneuver.

Using the available intent (21) and behavior preference (22), if $\mathbf{X}(t_k)$ is in the set $\mathcal{P}_{\mathrm{g}}^{\mathrm{A}}$ or in the set $\mathcal{P}_{\mathrm{g}}^{\mathrm{H}}$ then the ego vehicle shall pursue the merge ahead opportunity; otherwise it shall yield to the approaching remote vehicle to avoid potential conflicts. This is summarized in the decision-making rule

$$\text{decision} = \begin{cases} \text{merge ahead}, & \text{if } \mathbf{X}(t_k) \in \mathcal{P}_{\mathrm{g}}^{\mathrm{A}} \text{ or } \mathbf{X}(t_k) \in \mathcal{P}_{\mathrm{g}}^{\mathrm{H}}, \\ \text{yield}, & \text{otherwise.} \end{cases} \tag{23}$$

The following two Theorems provide criteria to check $\mathbf{X}(t_k) \in \mathcal{P}_{\mathrm{g}}^{\mathrm{A}}$ (for an automated ego vehicle) and $\mathbf{X}(t_k) \in \mathcal{P}_{\mathrm{g}}^{\mathrm{H}}$ (for a human-driven ego vehicle), respectively.

Theorem 1: Given the dynamics (16)-(17), the current system state $\mathbf{X}(t_k)$, the remote vehicle's latest available intent (21), and the behavior preference (22) of an ***automated*** *ego vehicle, we have*

$$\mathbf{X}(t_k) \in \mathcal{P}_{\mathrm{g}}^{\mathrm{A}} \iff T_0^{\mathrm{A}} < T_1, \tag{24}$$

where T_0^{A} is the time such that $r_0(T_0^{\mathrm{A}}) = -s$ under

$$u_0(t) \equiv \overline{a}_0(t), \quad t \geq t_k, \tag{25}$$

and T_1 is the time such that $r_1(T_1) = 0$ under

$$u_1(t) = \begin{cases} \overline{a}_1(t), & \text{if } t \in [t_k, \hat{t}_k + T], \\ a_{\max,1}, & \text{otherwise.} \end{cases} \tag{26}$$

Proof: See Appendix B. □

Theorem 2: Given the dynamics (16)-(17), the current system state $\mathbf{X}(t_k)$, the remote vehicle's latest available

intent (21), and the behavior preference (22) of a ***human-driven*** *ego vehicle, we have*

$$\mathbf{X}(t_k) \in \mathcal{P}_{\mathrm{g}}^{\mathrm{H}} \iff T_0^{\mathrm{H}} < T_1, \tag{27}$$

where T_0^{H} *is the time such that* $r_0(T_0^{\mathrm{H}}) = -s$ *under*

$$u_0(t) \equiv \underline{a}_0(t), \quad t \geq t_k, \tag{28}$$

while T_1 *is the same as in Theorem 1.*

Proof: See Appendix C. □

As depicted in Fig. 4(b), T_0^{A} in Theorem 1 calculates the time of an automated ego vehicle 0 exiting the conflict zone under its best-case behavior (input upper bound). In comparison, T_0^{H} in Theorem 2 corresponds to the time when a human-driven ego vehicle exits the conflict zone under its worst-case behavior (input lower bound) due to the uncertainty in human behavior. On the other hand, T_1 gives the time of the remote vehicle 1 entering the conflict zone under its worst-case future behavior, that is, when using the input upper bound in its intent (21) and in its physical behavior limits (17). As indicated by (26), with intent information, the ego vehicle can estimate the evolution of its environment with reduced uncertainty. It will be shown later experimentally that sharing intent significantly improves the efficiency in decision making. Notice that if $t_k \geq \hat{t}_k + T$ happens due to short intent horizon and/or improper communication conditions, then the intent is no longer available at t_k and (26) degrades to $u_1(t) \equiv a_{\max,1}$ for $t \geq t_k$.

Based on Theorems 1 and 2, examining $\mathbf{X}(t_k) \in \mathcal{P}_{\mathrm{g}}^{\mathrm{A}}$ or $\mathbf{X}(t_k) \in \mathcal{P}_{\mathrm{g}}^{\mathrm{H}}$ (i.e., whether a conflict-free merge ahead is guaranteed for an automated or a human-driven ego vehicle) reduces to calculating the time parameters T_0^{A}, T_0^{H}, and T_1. Such calculation can be done efficiently by performing numerical integration for the corresponding dynamics model using the indicated (deterministic) control inputs while satisfying output constraints. In the next section, we implement this intent-based conflict analysis algorithm on production vehicles to provide real-time decision assistance to human drivers.

IV. Experiments at the Mcity Test Track

In this section, we first discuss the implementation of vehicle intent (defined in Section II) in V2X messages. Then we present the experimental results obtained on a closed test track. These experiments validate the intent-based conflict analysis using connected vehicles. Experimental data is used to quantify the benefits of receiving intent messages.

A. Creating Intent Messages

We encode the longitudinal motion intent of Definition 2 into wireless messages using commercially available V2X communication devices; see Fig. 5(a). For simplicity, we focus on constant intent bounds for both acceleration (input) and velocity (output). The vehicle's longitudinal intent is packaged into a few parameters, which requires small data space to store and transmit, and uses communication resources efficiently. For time-dependent intent bounds, one may still parameterize them as functions of time to enable compact representation. Such implementation is left as future work.

(a) V2X OBU

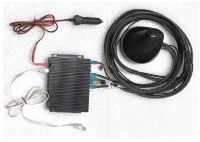

(b) Intent message example 1: cruise control

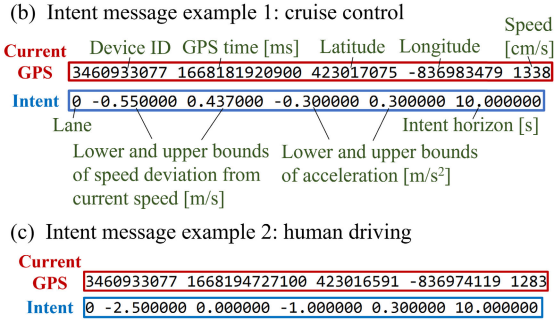

(c) Intent message example 2: human driving

Fig. 5. Implementing intent messages using the V2X protocol WSMP. (a) Commercially available V2X Onboard Unit (OBU). (b)-(c) Examples of intent messages transmitted in the experiments.

To implement intent messages, we adopt the WAVE Short Message Protocol (WSMP) [30], an efficient network layer messaging protocol that is able to transmit custom messages with standardized security [31]. Using the V2X Onboard Units (OBUs) shown in Fig. 5(a), we create secured intent messages in C language via the OBU supplier's application programming interface (API). We design appropriate data structures to store the intent parameters and specify the sending rate of intent packets. By running the developed C program on a computer connected to the OBU via Ethernet, intent messages can be sent/received by the OBU at a user-determined rate.

Two of intent message examples, corresponding to two different driving scenarios in our experiments are shown in Fig. 5(b)-(c). They were transmitted from a vehicle during a driving test whose details are given in the next subsection. The vehicle's current GPS information and its intent over a future horizon of 10 [s] are included in each message. Note that the intended velocity bounds are expressed relative to the current velocity of the vehicle. For instance, the intent message in Fig. 5(b) encodes a velocity range of $[13.38 - 0.55, 13.38 + 0.437]$ [m/s]. Examples of such intent bounds can be seen in Fig. 6(c)-(d). Thanks to the data-compact description of vehicle intent, the messages are contained in small packets of the size 51 bytes. One may further downsize intent packets by using data types that occupy less storage. Such lightweight design is important since smaller packet size contributes to less packet drops in real traffic [32].

B. Experiments at Mcity

Having implemented intent messages, we test intent sharing for conflict resolution using two human-driven vehicles equipped with V2X OBUs; see Fig. 5(a). Each OBU is equipped with a GPS unit, gyroscope, accelerometer, and magnetometer. Our OBUs communicate in a peer-to-peer manner through V2X antennas, using Cellular-V2X (C-V2X) direct communications [33]. Such C-V2X adopts an efficient wireless access technology – single carrier frequency division multiple access (SC-FDMA) at the medium access control

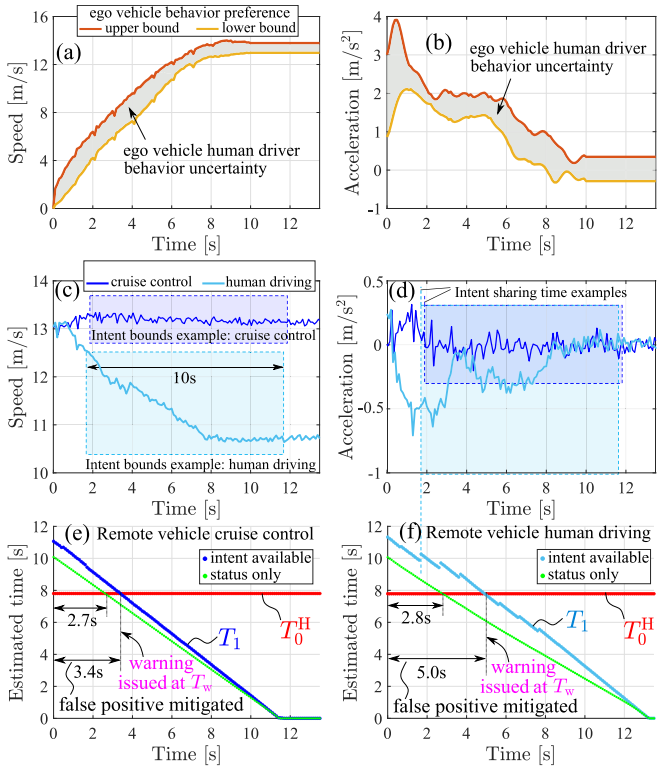

Fig. 6. Benefits evaluation of intent sharing in Mcity experiments where the ego vehicle performed on-board conflict analysis while maintaining standstill. (a)-(b) Ego vehicle's behavior preference. (c)-(d) Remote vehicle's maneuvers while using cruise control and when the human driver decreases the speed. Examples of intent bounds are highlighted as blue shadings. (e)-(f) Evolution of estimated times T_0^{H} and T_1 under the aforementioned two different behaviors of the remote vehicle. The warning issuance times T_{w} highlight the benefits of intent sharing in mitigating false positive decisions.

(MAC) layer [34], contributing to good communication range and reliability. During the tests, our OBUs operated at the 5.9 GHz frequency band with 20 dBm transmit power.

The experiments were performed at the Mcity test track of the University of Michigan. Fig. 4(a) shows the experimental setup, in which the ego vehicle (white) intends to merge onto the main road inside a 50 [m] long merge zone as the remote vehicle (blue) approaches on the main road. Notice that the merge zone does not exactly correspond to that of the actual on-ramp. Such design allows a longer section of the main road to be used by the remote vehicle to perform the required maneuvers (as specified below) before the ego vehicle merges. We define a conflict zone of length 20 [m]. To avoid danger to the experiment participants while studying conflicts, the second to the rightmost lane was used by the remote vehicle when approaching on the main road.

We define the initial time of each merge experiment as the moment when the distance between the remote vehicle and the conflict zone's entry point is 150 [m]. The ego vehicle's initial position is set at the entry point of the merge zone (30 [m] in front of the entry of the conflict zone), while its initial speed is set as zero; see Fig. 4(a). Such experimental setup replicates one of the most challenging merge scenarios where a merge has to be initiated from standstill; see Fig. 10(a)-(b) for a public road example that is often seen on US expressways. Note, however, that our methodology and qualitative results can be extended to many other traffic scenarios.

Two different behaviors were exhibited by the remote vehicle when driving along the main road: (i) cruise control with speed set to 30 [mi/hr] $\approx$ 13.4 [m/s]; (ii) human driving with speed decreasing from 30 [mi/hr]. Accordingly, we created intent messages for these two scenarios with the intent parameters given in the examples in Fig. 5(b)-(c). Examples of the remote vehicle's speed and acceleration profiles when performing such maneuvers are shown in Fig. 6(c)-(d). Blue shadings indicate the intent bounds which were determined based on data collected while the vehicle repeatedly performed such maneuvers. Indeed in practice, the parameters of human driving intent may be determined based on such historical data. The consideration of different remote vehicle behaviors allow us to demonstrate personalized decision assistance while responding to different intent information. The sending rate of intent messages was set to 1 [message/s]. Meanwhile, we used standard BSMs to transmit the remote vehicle's status information (position r_1 and velocity v_1) in every 0.1 [s].

In our experiments, the ego vehicle was human driven. We extracted the human driver's behavior preference beforehand by collecting data of the driver performing merge maneuvers multiple times at the test track. The cumulative min/max values of the speed and acceleration profiles yield the lower/upper bounds of the driver's preferred behavior shown in Fig. 6(a)-(b). The uncertainty in human driving is highlighted by the gray region between the bounds. Inside the ego vehicle, we used a computer to manage the reception of status and intent messages. The conflict analysis algorithm in Theorem 2 was implemented through MATLAB real-time. Decision assistance to the ego vehicle's human driver was provided on-board based on the decision rule (23) and Theorem 2, that is,

$$\text{decision assistance} = \begin{cases} \text{no warning}, & \text{if } T_0^{\mathrm{H}}(t_k) < T_1(t_k), \\ \text{warning issued}, & \text{if } T_0^{\mathrm{H}}(t_k) \geq T_1(t_k), \end{cases} \tag{29}$$

where t_k is status receiving time. Warning was issued from the computer running conflict analysis as audible beep sounds with a corresponding warning message displayed on the screen.

We performed experiments in two different ways. In the first case, highlighted in Figs. 4(a) and 6(e)-(f), on-board conflict analysis was performed while the ego vehicle stayed stationary at its initial position. These experiments were used to demonstrate the utility of intent sharing in resolving conflicts, and to quantify the benefits of intent. In the second case, shown in Fig. 7, on-board conflict analysis was performed while the ego vehicle's driver was asked to initiate the merge maneuver with different timings before/after the issuance of warning. These experiments enabled the validation of the intent-based conflict analysis for real human drivers' merge maneuvers. The results of these two categories of experiments are presented in detail in the next two subsections.

C. Evaluating Benefits of Intent Sharing

An experiment performed with stationary ego vehicles is illustrated in Fig. 4(a) through the ego vehicle's rear view camera images. With the remote vehicle being far away, the

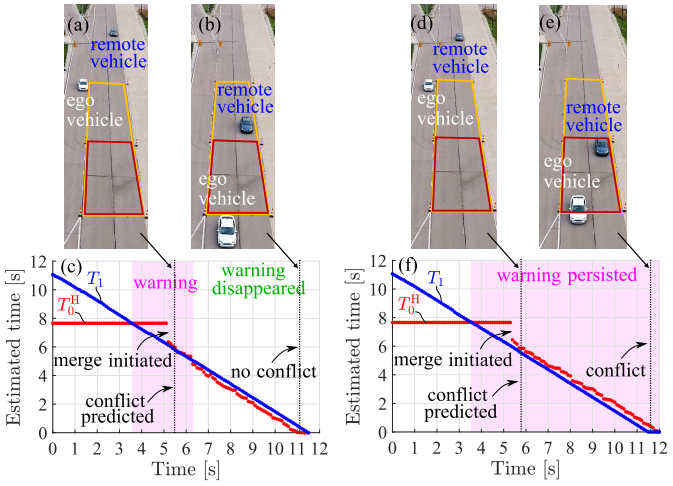

Fig. 7. Two examples of Mcity experiments where the remote vehicle approaches with cruise control and the ego vehicle driver merges after the issuance of warning. (a)-(c) A scenario where the warning disappeared automatically during the maneuver based on the ego vehicle's actual behavior and the updated V2X messages. No conflict happened after all as illustrated in panel (b). (d)-(f) A scenario where the warning persisted after being issued. Here an actual conflict happened as shown in panel (e).

on-board conflict analysis did not predict a conflict upon the ego vehicle merging ahead, and accordingly, no warning was issued. As the remote vehicle approached the ego vehicle from behind, a potential conflict between the two vehicles was predicted for the merge. Thus, a warning was generated, which continued until the remote vehicle passed the ego vehicle. Fig. 6(e)-(f) visualize the conflict analysis of two such experiments under the aforementioned two different behaviors of the remote vehicle (cruise control and human driving). Each time when a status update was received, the time parameters T_0^{H} and T_1 were calculated utilizing the ego vehicle's behavior preference and the remote vehicle's latest intent and status information. The small jumps (appearing every 1 [s]) in T_1 in Fig. 6(f) correspond to receiving new intent messages.

In what follows, we discuss the benefits quantification of intent sharing based on experimental results. To start, note that an ideal decision assistance shall (i) avoid *false negative* decisions, i.e., a conflict happens while a warning is not provided in time; (ii) minimize *false positive* decisions, i.e., a warning is provided while the ego vehicle can still confidently merge ahead without a conflict. Since our framework considers the worst-case behaviors of the remote and ego vehicles (see Theorem 2), the absence of *false negative* decisions is guaranteed theoretically, and this is also demonstrated empirically in the next subsection. Thus, mitigating *false positive* decisions is of our main interest. This is related to the *warning issuance time*, which is the time when the warning first appears after the experiment is initiated. A too early warning can lead to the human driver missing the opportunity to pursue a non-conflicting merge ahead, making the driver wait longer than necessary. Such unnecessary delays compromise the efficiency of the on-ramp.

According to (29) warnings are issued when $T_0^{\mathrm{H}} \geq T_1$. Thus, to quantify the benefits, we use the warning issuance time

$$T_{\mathrm{w}} = \min t_k \in \{t_0, t_1, \ldots\}, \quad \text{s.t.} \quad T_0^{\mathrm{H}}(t_k) \geq T_1(t_k), \tag{30}$$

where t_k are the times when status are received. In Fig. 6(e) and (f) we have $T_{\mathrm{w}} = 3.4$ [s] for the cruise control scenario and $T_{\mathrm{w}} = 5.0$ [s] for the human-driving scenario, respectively.

To highlight the benefits of intent sharing, we compare the warning issuance time T_{w} with a baseline case: when only status sharing messages are used. Suppose that intent messages had not been transmitted, the time parameter T_1 would be calculated with smaller values due to more conservative prediction on the remote vehicle's future behavior; see green curves in Fig. 6(e)-(f). In both cases, the warning issuance times shrink (to $T_{\mathrm{w}} = 2.7$ [s] and 2.8 [s], respectively). Therefore, intent sharing indeed mitigates *false positive* decisions in conflict resolution compared to status sharing.

Notice that for status sharing only, the difference between the warning issuing times associated with the cruise control and human driving cases is small. This is because of the similar status of remote vehicle at the beginning of both maneuvers. In contrast, with the anticipation of future motion encoded in the intent messages, different remote vehicle behaviors (intentions) were distinguished by our framework through the different warning issuing times.

D. Validating Intent-Based Conflict Analysis

Here we describe the experiments when the ego vehicle's human driver started to merge with designated timings before/after the issuance of the warning, while conflict analysis was performed. These experiments demonstrate that our framework enhances the safety of the ego vehicle by providing on-board warnings with no *false negative* decision and that the algorithm can self-correct the *false positive* decision in real-time during a merge.

In the experiment shown in Fig. 7(a)-(c), the remote vehicle was using cruise control while the ego vehicle's driver initiated the merge after the warning started. As panel (c) depicts, the value of T_0^{H} dropped at around 5.4 [s] when the ego vehicle began to move (whose actual behavior was better than the worst-case input used for conflict analysis). Then the on-board warning automatically disappeared during the maneuver at around 6.3 [s] based on the updated status and intent information. As shown in panel (b) conflict did not happen after all. Such self-adjustment of the warning showcased our framework's capability of real-time decision assistance. Another experiment is shown in Fig. 7(d)-(f), where the remote vehicle attempted to merge ahead amid the warning (which persisted throughout the maneuver), and this led to an actual conflict under the behavior uncertainty of the ego driver. We emphasize again that the warning was tailored to the specific driver's behavior preference.

By varying the ego vehicle's merge initiation timing, the experiments were repeated multiple times. For the case of cruise control, the experimental results are summarized in Fig. 8(a), depicting the ego vehicle's merge starting time and the remote vehicle's corresponding position, and representing the merge results by colors. As shown by the blue points, the ego vehicle was always able to merge ahead without a conflict when initiating a merge before the warning was issued, i.e., no *false negative* decision was observed. On the other hand,

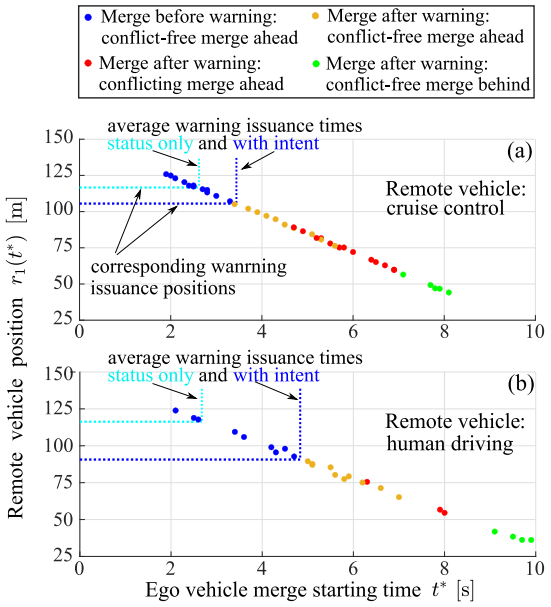

Fig. 8. Experimental results validating the on-board decision assistance enabled by intent-based conflict analysis. Each data point marks an experiment, showing the merge starting time of the ego vehicle and the corresponding position of the remote vehicle. Colors indicate different merge results. (a) Remote vehicle used cruise control. (b) Remote vehicle was human-driven.

the yellow points correspond to *false positive* decisions, which stem from using the ego drivers' worst-case behaviors when dealing with the uncertainties in human driving. Intent sharing indeed reduces such *false positive* decisions as highlighted by the larger average warning issuance times, compared to the status sharing only case. Such *false positive* warnings were self-corrected in real-time during the maneuver based on the updated information; see Fig. 7(a)-(c). The necessity of having conservatism in conflict analysis is, however, justified by a segment of data points with mixed yellow and red colors in Fig. 8(a), that is, conflicts could occur depending on the ego driver's actual behavior. With the remote vehicle being closer, merge ahead was no longer achievable without a conflict, as shown by the red points. Finally, the green points indicate that, by following the warning, a conflict-free merge behind was always realizable.

As shown in Fig. 8(b), when the remote vehicle was operated by a human driver, the experimental results remained qualitatively similar. In fact, the on-board warning system was also tested under a different human driver of the ego vehicle, who drove more aggressively (with higher values of the preferred velocity and acceleration bounds). While the detailed results of such experiments are omitted in this paper due to qualitative similarity, we observed larger warning issuance times due to a more aggressive behavior preference. These experiments validated the capability of the conflict analysis in providing personalized decision assistance tailored to different ego drivers under different remote vehicle intentions. We demonstrated that the real-time on-board warning provided a sufficient safety margin in alerting the human driver of the ego vehicle of a potential conflict. At the same time our intent-based warning leads to a significant reduction in *false positives* compared to a status-based warning.

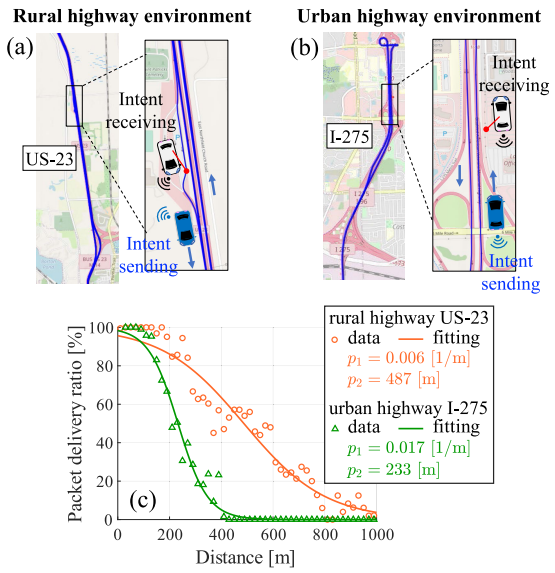

Fig. 9. Testing packet delivery ratio of intent messages (a) on a rural section of highway US-23, and (b) on an urban section of highway I-275. (c) The corresponding packet delivery ratios as a function of distance between intent sender and receiver.

V. Evaluating Intent Sharing Using Highway Data

So far we validated intent sharing at the Mcity test track. In this section we bring intent sharing to public roads. We first test intent messages on real highways. Then we perform numerical simulations to investigate the effects of communication conditions on the benefits of intent sharing.

A. Packet Delivery Ratios on Public Highways

The transmission of intent messages was tested using connected human-driven vehicles on two different highways in southeast Michigan: on a rural section of highway US-23; and on an urban section of highway I-275.

The experimental setup used on highway US-23 is depicted in Fig. 9(a). While traveling along the highway, the blue vehicle sent status messages via BSMs and intent messages as described in Section IV-A, both at a rate of every 0.1 [s]; see the blue trajectory for the route taken. The white vehicle received the messages while staying next to the highway at a rest area. The collected data allowed for the calculation of intent packet delivery ratio, i.e., the percentage of packets received versus those have been sent, under different inter-vehicle distances. Note that here we are interested in testing the intent packet reception on public roads, while the exact intent parameter values in each message are not important. Similar experimental setup is shown in Fig. 9(b) for the experiments conducted on an urban section of highway I-275.

The reception of intent packets was indeed affected by the distance and the environment in which the vehicles were operating; see data points in Fig. 9(c). To capture the trend of decreasing packet delivery ratio as a function of the inter-vehicle distance d, we fit the sigmoid function

$$S(d) = 1 - \frac{1}{1 + e^{-p_1(d-p_2)}}, \tag{31}$$

to the data where parameter p_1 describes the decreasing rate (steepness) while parameter p_2 corresponds to the d value at the function's midpoint. Such function has been widely used in the literature for evaluating wireless messages' packet delivery ratios [35]. To fit the function (31) to the data, we minimize the root mean square error

$$\text{RMSE} = \sqrt{\frac{1}{M}\sum_{k=1}^{M}\left(S(d_k) - \hat{S}_k\right)^2}, \tag{32}$$

where $d_1, \ldots, d_M$ represent distances where packet delivery ratio data $\hat{S}_1, \ldots, \hat{S}_M$ are available. The fitted functions are depicted as solid curves in Fig. 9(c) with the corresponding parameter values shown on the right.

For the rural highway section on US-23, relatively high packet delivery ratio is maintained until 200 [m], while gradual drops appeared for larger distances. Notice that intent packets could be received up to 1000 [m]. For the urban highway environment on I-275, the packet delivery ratio drops earlier and more sharply as inter-vehicle distance increases; see larger p_1 and smaller p_2 values. This deterioration is due to obstructions such as dense traffic, buildings and overpasses. We remark that these observations are representative – our further tests revealed more intent packet drops on urban roads compared to urban highways, due to more obstacle-related communication interruptions. The qualitative trend, however, remains similar. On the other hand, the packet delivery ratio in the Mcity experiments (Fig. 7) was almost 100% due to the small size of the test track.

These data-based results of packet delivery ratio will be used in the next subsection to evaluate the effects of communication conditions on the benefits of intent sharing in resolving conflicts for cooperative maneuvers.

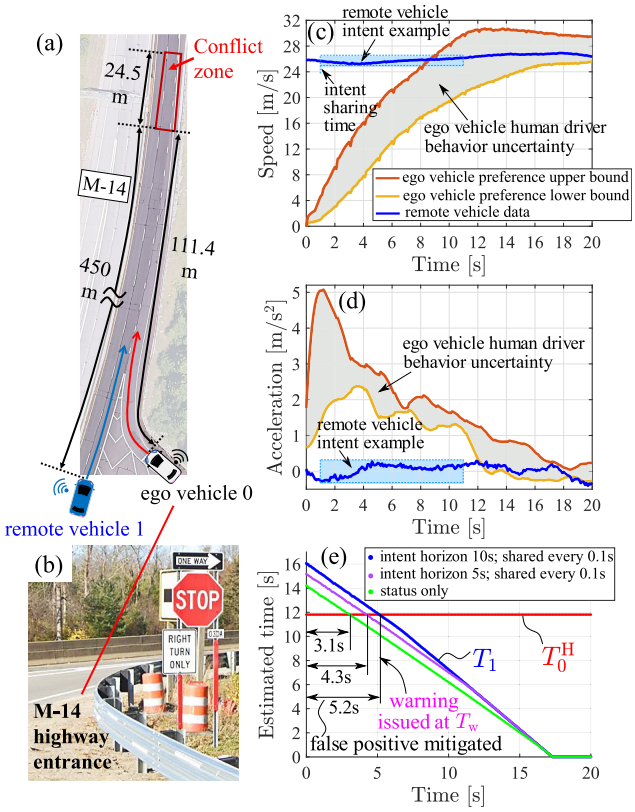

Fig. 10. Data-based simulation of a merge scenario at the on-ramp of highway M-14 near Barton Drive, Ann Arbor, Michigan. (a)-(b) Simulation setup where the ego vehicle merges from a stop sign. (c)-(d) The ego vehicle's behavior preference and remote vehicle's speed profile (extracted from a real human driver data). (e) Conflict analysis showing the estimated times T_0^{H} and T_1. The warning issuance times are highlighted for different intent sending conditions.

B. Effects of Communication Conditions

In this subsection, we study the benefits of intent sharing under imperfect communication where intent packet drops exist, while considering different intent sending conditions (e.g., rate and horizon). To this aim, we perform numerical simulations for a highway merge scenario in a real-world road configuration using real human driving data. We select the on-ramp of highway M-14 near Barton Drive in Ann Arbor, Michigan, as our simulation example, which requires a highway merge to be initiated from a stop sign with zero initial speed; see Fig. 10(a)-(b). For this highway merge section, we define a conflict zone shown as the red rectangle in Fig. 10(a). The entry point of the conflict zone is where the lane width of the on-ramp shrinks to 1.2 [m], which is narrower than a typical vehicle and a conflict with adjacent lane vehicles becomes apparent. The conflict zone ends at the end of the ramp. This yields a conflict zone size of 24.5 [m]. We remark that when choosing a slightly different start/end points for the conflict zone the simulation results remain similar.

We consider the scenario that a human-driven ego vehicle attempts to merge from standstill at the highway entrance, while a remote vehicle is approaching along the rightmost lane. To obtain behavior preference of a human driver's merge maneuver, we collected data from a driver who merged multiple times from the M-14 entrance. Similar to the Mcity experiments, we extracted the lower/upper bounds of preferred speed and acceleration shown in Fig. 10(c)-(d). The initial position of the ego vehicle (at the stop sign) is 111.4 [m] away from the entry point of the conflict zone. To represent the remote vehicle's behavior for the simulation, we use data collected by a human-driven vehicle; see the blue curves in Fig. 10(c)-(d). The initial position of remote vehicle is selected as 450 [m] from the conflict zone. That is, the two vehicles are (roughly) 338.6 [m] apart at the initial time, enabling the exchange of intent messages (with packet drops); cf. Fig. 9(c).

In the simulation, the remote vehicle shares its status (position and speed) every 0.1 [s], while the intent information (of Definition 2) is shared with different sending rates and intent horizons. At any intent sharing time, the bounds of the intended speed and acceleration are extracted from the remote vehicle's data. The blue shadings in Fig. 10(c)-(d) illustrate an example of intent shared at 1 [s] with a horizon of 10 [s], where the min/max values of the corresponding data segment yield the bounds. Note that in reality intent may not be generated this way as one does not know exactly the future profile, but simulations with such "accurate" intent allow us to focus on investigating the effects of communication conditions.

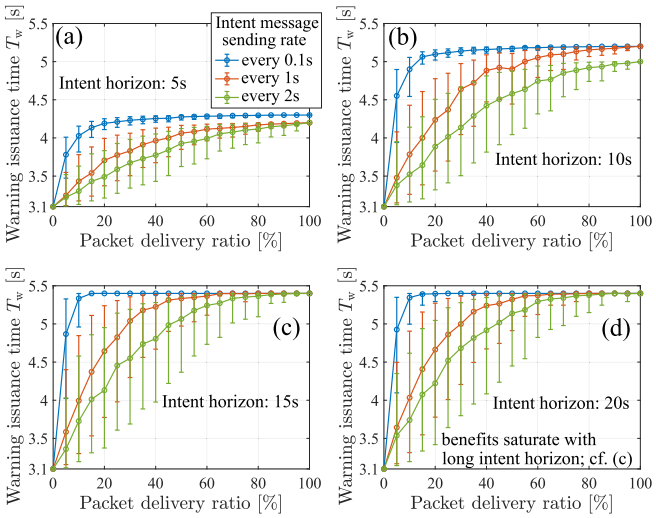

Fig. 11. Evaluating the effects of communication conditions (intent horizon, sending rate, and packet delivery ratio) on the benefits of intent sharing via simulations. The warning issuance time is plotted as a function of packet delivery ratio with the indicated intent horizons and sending rates. The dots mark mean values while the error bars show the standard deviations.

As the remote vehicle approaches, the ego vehicle performs on-board conflict analysis while staying at the stop sign. Corresponding to highway driving, the speed limits of the remote vehicle are set as $v_{\min,1} = 20$ [m/s] and $v_{\max,1} = 32$ [m/s], while its acceleration limits are the same as in Table I. The simulation results in Fig. 10(e) show the estimated times T_0^{H} and T_1 calculated via conflict analysis. Here, we incorporated the intent packet delivery ratio of the rural highway US-23 (orange curve in Fig. 9(c)) into the simulation. Namely, the reception of intent packets is modeled by a Bernoulli process such that the probability of receiving a packet is given by the packet delivery ratio corresponding to the current distance between vehicles.

Three different intent sharing conditions are simulated for the remote vehicle. Without intent sharing (green curve), the warning starts at $T_{\mathrm{w}} = 3.1$ [s]. When intent is sent every 0.1 [s] with horizon 5 [s] (purple curve), the warning starts later at $T_{\mathrm{w}} = 4.3$ [s], giving more opportunity for the ego vehicle to pursue merge ahead. As the intent horizon is increased to 10 [s] while maintaining the same sending rate, the warning issuance time is pushed to $T_{\mathrm{w}} = 5.2$ [s]. Such improvement is because longer intent horizon enables a more accurate (less conservative) prediction of the remote vehicle's future maneuver; cf. (26). Thus, longer intent horizon boosts the time efficiency of the ego vehicle (and those queuing behind it). Simulations with a worse packet delivery ratio associated with the urban highway I-275 (green curve in Fig. 9(c)) yield slightly smaller warning issuance times, but the qualitative trend remains similar.

To further quantify the effects of communication conditions, we repeat the simulations for different values of packet delivery ratio under different sending rates and intent horizons. Here we adopt the simplification that packet delivery ratio is independent from the inter-vehicle distance. Fig. 11(a) plots the warning issuance time T_{w} as a function of packet delivery ratio for intent horizon 5 [s] with the three sending rates as indicated. Each dot marks the mean value of 500 simulations while error bars represent standard deviations. The latter are calculated separately above and below the mean to reflect more accurate distribution. For sending rate 0.1 [s] (blue curve), the warning issuance time remain almost constant between $20 - 100\%$ packet delivery ratios, indicating that intent sharing has good tolerance against packet drops. For lower sending rates (orange and green curves), the system becomes less resilient to packet loss as shown by the lower mean values and higher variance. Having higher sending rate boosts the chance of the ego vehicle obtaining an intent packet, which can provide information regarding its future environment.

The intent horizon also affects the merge performance significantly. When the horizon is increased to 10 [s] as in Fig. 11(b), the warning issuance times witness a significant increase, while the qualitative trends remain similar. As the horizon is increased further to 15 [s] as in Fig. 11(c), we observe further (but moderate) increase in warning issuance times and improved tolerance to packet drops. These benefits eventually saturate as shown in Fig. 11(d) for horizon 20 [s] which is long enough to cover the rest of the merge maneuver.

The above data-based simulations enable a systematic evaluation of communication factors in intent sharing. These results provide insights into designing efficient generation rules of intent messages. For instance, an adaptive transmission rate may be imposed such that under reliable communication, long-horizon intent is sent with lower rate to save communication channels while maintaining comparable performance; cf. Fig. 11(c)-(d). Our studies are expected to benefit standardization and future deployments.

VI. Conclusion

In this paper, we proposed a generalized representation of vehicle motion intent from a system dynamics viewpoint. We extended conflict analysis to incorporate intent information for conflict resolution for an ego vehicle (which may be either automated or human-driven), while considering user-determined behavior preference. We implemented and tested intent messages using real vehicles equipped with commercially available V2X devices. An on-board decision assistance system was developed and validated through experiments at a test track to facilitate the decision-making of human drivers in merge scenarios. It was shown that such system can provide individualized assistance to human drivers while utilizing intent information. Experimental results demonstrated that receiving intent messages, in addition to status information, can significantly improve a vehicle's safety and time efficiency in cooperative maneuvers, by mitigating the uncertainty of its future environments. Furthermore, highway data was used together with numerical simulations to investigate the effects of communication conditions (e.g., intent sending rate, horizon, and packet drops) on the obtained benefits.

In the future, we will design intent messages containing more sophisticated motion information. We will also implement intent messages in an adaptive manner, where a vehicle's intent will be updated online according to real-time traffic and communication conditions. Moreover, our intent-based conflict analysis will be extended to accommodate the existence

of non-connected vehicles. In the absence of connectivity, vehicles' status and intent information may be estimated through perception, which is expected to be less accurate and computationally more expensive than V2X-based status and intent information. The corresponding impact on traffic safety and efficiency will be investigated. Our experimental study will also be extended to automated vehicles and higher levels of cooperation.

APPENDIX A
PROOF OF THE RELATIONSHIP (19)

For simplicity of notation, we define a proposition

$$Q := \{r_0(t) \geq -s \wedge -s \leq r_1(t) \leq 0\}, \tag{33}$$

then (19) becomes $P \iff \{\forall t, \neg Q\}$.

We first prove $P \implies \{\forall t, \neg Q\}$. If $P =$ true, then according to definition (18), one can find such a time $t = \bar{t}$ that $r_0(\bar{t}) < -s \wedge r_1(\bar{t}) = 0$ holds. This yields immediately $\neg Q =$ true at such $\bar{t}$. Since the vehicles do not move backward, for any given $t > \bar{t}$, $r_0(t) < -s$ still holds, while for any given $t < \bar{t}$, one has $r_1(t) > 0$. Therefore, $\neg Q =$ true also holds for any $t \neq \bar{t}$. These lead to $\{\forall t, \neg Q\}$.

To show $P \impliedby \{\forall t, \neg Q\}$, we prove its contrapositive, i.e., $\neg P \implies \{\exists t, Q\}$. From (18) we have $\neg P = \{\forall t, r_0(t) \geq -s \vee r_1(t) \neq 0\}$. Since $r_1(t)$ monotonically decreases along t with $\dot{r}_1 \leq -v_{\min,1} < 0$, there must exist a time $\tilde{t}$, such that $r_1(\tilde{t}) = 0$. If $\neg P =$ true, then at such $\tilde{t}$ we have $r_0(\tilde{t}) \geq -s$. Hence, $\neg P \implies \{\exists t = \tilde{t}, r_0(\tilde{t}) \geq -s \wedge r_1(\tilde{t}) = 0\} \implies \{\exists t, Q\}$. These complete the proof of (19).

APPENDIX B
PROOF OF THEOREM 1

The relationship (24) is shown below.

($\implies$). We prove its contrapositive, i.e., $\mathbf{X}(t_k) \notin \mathcal{P}_g^A \impliedby T_0^A \geq T_1$. If $T_0^A \geq T_1$, then for any admissible input u_0, we have $\bar{T}_0^A \geq T_0^A \geq T_1$, where $\bar{T}_0^A$ represents the time such that $r_0(t) = -s$ under the given u_0. Thus, $\exists u_1$ in (26), $\forall u_0$, $r_0(T_1) \geq r_0(\bar{T}_0^A) \geq -s \wedge r_1(T_1) = 0$, implying $\{\exists t = T_1, Q\}$, where proposition Q is defined by (33) in Appendix A. Based on (19), we have $\exists u_1, \forall u_0, \neg P$, that is, $\mathbf{X}(t_k) \notin \mathcal{P}_g^A$.

($\impliedby$). If $T_0^A < T_1$, then for any admissible input u_1, we have $T_0^A < T_1 \leq \bar{T}_1$, where $\bar{T}_1$ represents the time such that $r_1(t) = 0$ under the given u_1. Thus, $\forall u_1$, $\exists u_0$ in (25), $r_0(\bar{T}_1) < r_0(T_0^A) = -s \wedge r_1(\bar{T}_1) = 0$. That is, $\forall u_1, \exists u_0, P$, i.e., $\mathbf{X}(t_k) \in \mathcal{P}_g^A$.

APPENDIX C
PROOF OF THEOREM 2

Below we prove the relationship (27).

($\implies$). If $\mathbf{x}(t_k) \in \mathcal{P}_g^H$, then for the inputs u_0 and u_1 in (28) and (26), we have $\exists t, r_0(t) < -s \wedge r_1(t) = 0$. Such t must be unique since $r_1(t)$ is monotonic along t, yielding $t = T_1$. Thus, $T_0^H < T_1$ holds obviously.

($\impliedby$). If $T_0^H < T_1$, then for the inputs u_0 and u_1 in (28) and (26), we have $r_0(T_1) < -s \wedge r_1(T_1) = 0$. For any admissible u_0 and u_1 other than (28) and (26), let $\bar{T}_0^H$ and $\bar{T}_1$ be the times such that $r_0 = -s$ and $r_1 = 0$. We have $\bar{T}_0^H < T_0^H < T_1 < \bar{T}_1$. Thus, $r_0(\bar{T}_1) < -s \wedge r_1(\bar{T}_1) = 0$. These imply $\mathbf{x}(t_k) \in \mathcal{P}_g^H$.

REFERENCES

[1] L. Hobert, A. Festag, I. Llatser, L. Altomare, F. Visintainer, and A. Kovacs, "Enhancements of V2X communication in support of cooperative autonomous driving," *IEEE Commun. Mag.*, vol. 53, no. 12, pp. 64–70, Dec. 2015.

[2] I. Llatser, T. Michalke, M. Dolgov, F. Wildschütte, and H. Fuchs, "Cooperative automated driving use cases for 5G V2X communication," in *Proc. 2nd IEEE 5G World Forum (5GWF)*, Sep. 2019, pp. 120–125.

[3] J. Jeong et al., "A comprehensive survey on vehicular networks for smart roads: A focus on IP-based approaches," *Veh. Commun.*, vol. 29, Jun. 2021, Art. no. 100334.

[4] A. I. M. Medina, N. van de Wouw, and H. Nijmeijer, "Automation of a T-intersection using virtual platoons of cooperative autonomous vehicles," in *Proc. IEEE 18th Int. Conf. Intell. Transp. Syst.*, Sep. 2015, pp. 1696–1701.

[5] C. Liu, C.-W. Lin, S. Shiraishi, and M. Tomizuka, "Distributed conflict resolution for connected autonomous vehicles," *IEEE Trans. Intell. Vehicles*, vol. 3, no. 1, pp. 18–29, Mar. 2018.

[6] J. Rios-Torres and A. A. Malikopoulos, "A survey on the coordination of connected and automated vehicles at intersections and merging at highway on-ramps," *IEEE Trans. Intell. Transp. Syst.*, vol. 18, no. 5, pp. 1066–1077, May 2017.

[7] R. Hult, M. Zanon, S. Gros, and P. Falcone, "Optimal coordination of automated vehicles at intersections: Theory and experiments," *IEEE Trans. Control Syst. Technol.*, vol. 27, no. 6, pp. 2510–2525, Nov. 2019.

[8] R. Kianfar, P. Falcone, and J. Fredriksson, "Safety verification of automated driving systems," *IEEE Intell. Transp. Syst. Mag.*, vol. 5, no. 4, pp. 73–86, Winter 2013.

[9] M. R. Hafner, D. Cunningham, L. Caminiti, and D. Del Vecchio, "Cooperative collision avoidance at intersections: Algorithms and experiments," *IEEE Trans. Intell. Transp. Syst.*, vol. 14, no. 3, pp. 1162–1175, Sep. 2013.

[10] S. Bansal, M. Chen, S. Herbert, and C. J. Tomlin, "Hamilton–Jacobi reachability: A brief overview and recent advances," in *Proc. 56th IEEE Conf. Decis. Control*, Dec. 2017, pp. 2242–2253.

[11] X. Di and R. Shi, "A survey on autonomous vehicle control in the era of mixed-autonomy: From physics-based to AI-guided driving policy learning," *Transp. Res. C, Emerg. Technol.*, vol. 125, Apr. 2021, Art. no. 103008.

[12] *Taxonomy and Definitions for Terms Related To Cooperative Driving Automation for On-Road Motor Vehicles*, Standard SAE J3216, 2020.

[13] *Taxonomy and Definitions for Terms Related To Driving Automation Systems for On-Road Motor Vehicles*, Standard SAE J3016, 2021.

[14] *Dedicated Short Range Communications (DSRC) Message Set Dictionary Set*, Standard SAE J2735, 2016.

[15] *Intelligent Transport Systems (ITS); Vehicular Communications; Basic Set of Applications; Part 2: Specification of Cooperative Awareness Basic Service*, Standard ETSI EN 302 637-2, V1.4.1, 2019.

[16] Y. E. Sahin, Z. Liu, K. Rutledge, D. Panagou, S. Z. Yong, and N. Ozay, "Intention-aware supervisory control with driving safety applications," in *Proc. IEEE Conf. Control Technol. Appl. (CCTA)*, Aug. 2019, pp. 1–8.

[17] M. Wu et al., "Gaze-based intention anticipation over driving manoeuvres in semi-autonomous vehicles," in *Proc. IEEE/RSJ Int. Conf. Intell. Robots Syst. (IROS)*, Nov. 2019, pp. 6210–6216.

[18] Y. Chen, N. Sohani, and H. Peng, "Modelling of uncertain reactive human driving behavior: A classification approach," in *Proc. IEEE Conf. Decis. Control (CDC)*, Dec. 2018, pp. 3615–3621.

[19] *Application Protocol and Requirements for Maneuver Sharing and Coordinating Service*, Standard SAE J3186, 2023. [Online]. Available: https://www.sae.org/standards/content/j3186/

[20] *Intelligent Transport Systems (ITS); Vehicular Communications; Informative Report for the Maneuver Coordination Service*, Standard ETSI TR 103 578, Feb. 2022.

[21] B. Lehmann, H.-J. Günther, and L. Wolf, "A generic approach towards maneuver coordination for automated vehicles," in *Proc. 21st Int. Conf. Intell. Transp. Syst. (ITSC)*, 2018, pp. 3333–3339.

[22] A. Correa et al., "Infrastructure support for cooperative maneuvers in connected and automated driving," in *Proc. IEEE Intell. Vehicles Symp. (IV)*, Jun. 2019, pp. 20–25.

[23] R. Molina-Masegosa, S. S. Avedisov, M. Sepulcre, Y. Z. Farid, J. Gozalvez, and O. Altintas, "V2X communications for maneuver coordination in connected automated driving: Message generation rules," *IEEE Veh. Technol. Mag.*, vol. 18, no. 3, pp. 91–100, Sep. 2023.
[24] R. Molina-Masegosa, S. S. Avedisov, M. Sepulcre, Y. Z. Farid, J. Gozalvez, and O. Altintas, "Insights into the design of V2X-based maneuver coordination for connected automated driving," in *Proc. IEEE 96th Veh. Technol. Conf. (VTC-Fall)*, Sep. 2022, pp. 1–5.
[25] R. van Hoek, J. Ploeg, and H. Nijmeijer, "Cooperative driving of automated vehicles using B-splines for trajectory planning," *IEEE Trans. Intell. Vehicles*, vol. 6, no. 3, pp. 594–604, Sep. 2021.
[26] H. M. Wang, S. S. Avedisov, T. G. Molnár, A. H. Sakr, O. Altintas, and G. Orosz, "Conflict analysis for cooperative maneuvering with status and intent sharing via V2X communication," *IEEE Trans. Intell. Vehicles*, vol. 8, no. 2, pp. 1105–1118, Feb. 2023.
[27] H. M. Wang, S. S. Avedisov, A. H. Sakr, O. Altintas, and G. Orosz, "Opportunistic strategy for cooperative maneuvering using conflict analysis," in *Proc. IEEE Intell. Vehicles Symp. (IV)*, Jul. 2021, pp. 348–353.
[28] H. M. Wang, S. S. Avedisov, O. Altintas, and G. Orosz, "Multi-vehicle conflict management with status and intent sharing under time delays," *IEEE Trans. Intell. Vehicles*, vol. 8, no. 2, pp. 1624–1637, Feb. 2023.
[29] H. M. Wang, S. S. Avedisov, O. Altintas, and G. Orosz, "Experimental validation of intent sharing in cooperative maneuvering," in *Proc. IEEE Intell. Vehicles Symp. (IV)*, Jun. 2023, pp. 1–6.
[30] *IEEE Standard for Wireless Access in Vehicular Environments (WAVE)—Networking Services*, Standard 1609.3, Dec. 2020.
[31] *IEEE Standard for Wireless Access in Vehicular Environments—Security Services for Applications and Management Messages*, Standard 1609.2, 2016.
[32] H. M. Wang, S. S. Avedisov, O. Altintas, and G. Orosz, "Evaluating intent sharing communication using real connected vehicles," in *Proc. IEEE Veh. Netw. Conf. (VNC)*, Apr. 2023, pp. 69–72.
[33] G. Cecchini, A. Bazzi, B. M. Masini, and A. Zanella, "Localization-based resource selection schemes for network-controlled LTE-V2V," in *Proc. Int. Symp. Wireless Commun. Syst. (ISWCS)*, 2017, pp. 396–401.
[34] B. M. Masini, A. Bazzi, and E. Natalizio, "Radio access for future 5G vehicular networks," in *Proc. IEEE 86th Veh. Technol. Conf. (VTC-Fall)*, Sep. 2017, pp. 1–7.
[35] M. Sepulcre, J. Gozalvez, B. Coll-Perales, M. C. Lucas-Estan, and J. R. Gisbert, "Empirical performance models for V2V communications," in *Proc. IEEE Int. Conf. Comput. Inf. Technol., Ubiquitous Comput. Commun., Dependable, Autonomic Secure Comput., Pervasive Intell. Comput.*, Oct. 2015, pp. 737–742.

Hao M. Wang received the B.Eng. degree in mechanical and aerospace engineering from Nagoya University, Nagoya, Japan, in 2018. He is currently pursuing the Ph.D. degree in mechanical engineering with the University of Michigan, Ann Arbor, MI, USA. His research interests include dynamics and control of connected and automated vehicles.

Sergei S. Avedisov (Member, IEEE) received the Ph.D. degree in mechanical engineering from the University of Michigan, Ann Arbor, MI, USA, in 2019. He is currently a Cooperative Automated Driving Engineer with Toyota Research and Development–InfoTech Labs. His research interests include cooperative automated driving, cooperative perception, cooperative maneuvering, vehicle-to-everything communications, and cooperative platooning in mixed traffic.

Onur Altintas received the Ph.D. degree in electronics engineering from The University of Tokyo. Since 1999, he has been with Toyota Group in various roles in New Jersey, Tokyo, and California. He is currently the InfoTech Labs Fellow and a Senior Executive Engineer with Toyota Motor North America Research and Development–InfoTech Labs. He has been the Co-Founder and the General Co-Chair of the IEEE Vehicular Networking Conference (IEEE VNC) since 2009. He serves as an Associate Editor for *IEEE Intelligent Transportation Systems Magazine*, *IEEE Vehicular Technology Magazine*, and IEEE TRANSACTIONS ON INTELLIGENT VEHICLES. He is an IEEE Vehicular Technology Society Distinguished Lecturer.

Gábor Orosz (Senior Member, IEEE) received the M.Sc. degree in engineering physics from Budapest University of Technology, Hungary, in 2002, and the Ph.D. degree in engineering mathematics from the University of Bristol, U.K., in 2006. He was a Post-Doctoral Researcher with the University of Exeter, U.K., and the University of California, Santa Barbara. In 2010, he joined the University of Michigan, Ann Arbor, MI, USA, where he is currently an Associate Professor in mechanical engineering and civil and environmental engineering. From 2017 to 2018, he was a Visiting Professor in control and dynamical systems with California Institute of Technology. In 2022, he was a Distinguished Guest Researcher in applied mechanics with Budapest University of Technology. His research interests include nonlinear dynamics and control, time delay systems, machine learning, and data-driven systems with applications to connected and automated vehicles, traffic flow, and biological networks.